International Journal of Development Mathematics Vol 2 Issue 4 Page No. 044 - 074

INTERNATIONAL JOURNAL OF DEVELOPMENT MATHEMATICS

ISSN: 3026-8656 (Print) | 3026-8699 (Online)

journal homepage: https://ijdm.org.ng/index.php/Journals

Mathematical Modeling and Optimal Control Analysis of Cholera Dynamics with Environmental Reservoir

Ayuba Sanda[a*], Mohammed S. Adamu[ab], Abubakar B. Muhammad[a], Yahaya Ajiya[a]

Alhassan Ibrahim[c]

[a]Department of Mathematical Sciences, Faculty of Science, Gombe State University, Gombe, Gombe State, Nigeria
[a]Department of General Studies, School of General and Remedial Studies, Federal Polytechnic Damaturu,, Yobe State, Nigeria
[s]School of Continuing Education , Bayero University, Kano, Kano State, Nigeria

ARTICLE INFO

Article history:
Received 02 August 2025
Received in revised form 10 November 2025
Accepted 20 November 2025

Keywords:
Cholera, optimal control, awareness, quarantine, treatment, environmental reservoir, cost-effectiveness
MSC 2020 Subject classification:
30C45.

ABSTRACT

The article investigates the dynamics of cholera transmission through the construction and analysis of a deterministic compartmental model. Some of the results obtained from the analysis are the derivation of the basic reproduction number $\mathcal{R}_0$, and the stability analysis of the disease-free and endemic equilibria. The sensitivity analysis shows that the most sensitive parameters is the ingestion rate (β), recruitment of susceptible (Λ). Numerical models reveal a steady increase in both symptomatic and asymptomatic infections and continued high bacterial environmental loads when there is no controlled. In contrast, if awareness, quarantine, and treatment controls are put together, then infection prevalence and environmental contamination are greatly reduced. Treatment has a great expense but results in fast reductions of the infection rate; awareness efforts are the most cost-effective as they promote precautionary measures that can help avoid the infection of cholera. Quarantine reduces secondary transmission, a vital supporting role. Cholera containment and eradication need long-term behavioral, quarantine, and treatments, something that is demonstrated within the integrated control framework.

1. Introduction

Cholera is a serious global health problem that leads to 21,000 to 143,000 deaths each year. It spreads mainly through contaminated water via fecal-oral routes. The environment can support outbreaks, making transmission sometimes indirect. Asymptomatic individuals can unknowingly increase environmental contamination. This makes it harder to control the disease. According to the World Health Organization (2017), the Global Task Force on Cholera Control aims to reduce cholera deaths by 90% and eliminate transmission in targeted countries by 2030.

Mathematical modelling is key to understanding how cholera spreads. It helps assess intervention strategies and guides responses to outbreaks. Recent models examine important factors like asymptomatic transmission, environmental reservoirs, vaccine effects, and the success of quarantine measures. A study by Al-Arydah et al. (2013) found that educating the public about the disease is more effective than water chlorination in reducing cholera infections and lowering the number of bacteria in the environment. Mukandavire et al. (2011) formulated a

* Corresponding author. Tel.: +2348065874739
E-mail address: ayubasanda@gsu.edu.ng (Ayuba Sanda)
https://doi.org/10.62054/ijdm/0204.03

compartmental model to study outbreaks in Zimbabwe and Haiti and they showed the need for specific interventions based on local conditions. Neilan et al. (2010) developed a model that includes key elements like short-lived hyper infectious bacterial states and specific categories for mildly symptomatic individuals. It also looks at waning immunity. Their findings serve as a helpful guide for creating effective control strategies. Posny et al. (2015) created a deterministic cholera model that includes treatment, vaccination, and sanitation efforts. Their model highlights that cholera is still a serious public health threat, especially in developing countries. They studied the dynamics and optimal control theory to identify cost-effective, time-sensitive interventions. Njagarah and Nyabadza (2015) built a model that looks at how cholera spreads between two communities. They considered specific reproduction numbers and human movement. They identified control variables and parameters that affect infection dynamics. Their model shows that coordinated efforts such as promoting hygiene, improving sanitation, and vaccinating can lessen the impact and severity of the disease. This approach could even result in quick eradication.

Lemos-Paião et al. (2016) designed a cholera model with quarantine compartments to reduce infections and bacterial loads while lowering the costs of interventions. Yang et al. (2017) proposed two models to study how human behavior and disease awareness programs influence cholera transmission. Song et al.'s study in 2020 demonstrated that combining vaccination and sanitation is more effective than any single method in controlling global transmission dynamics. Hezam et al. (2021) found that integrating disease-specific and general public health actions can reduce the overall disease burden in Yemen, especially given the concurrent spread of cholera and COVID-19. Helan et al. (2021) created a model to analyze the spread of both diseases in Yemen, evaluating control strategies such as social distancing, lockdowns, testing, and chlorine distribution for water. Their results showed that a combined approach significantly reduces infection rates and flattens epidemic curves.

Brown et al. (2021) developed a nonlinear SEIR model featuring three interventions: intensive treatment, screening, and self-protection induced by information. They concluded that screening alone is cost-effective, but using multiple strategies together lowers the disease burden and is more economical. Treatment works best for mild outbreaks, while screening is more impactful during severe epidemics. Berhe (2020) applied optimal control theory to examine cholera transmission in Ethiopia's Oromia Region. The parameters of the model, including the rate of Vibrio cholerae intake and recovery, are crucial for understanding disease spread. The study indicates that treatment is the most cost-effective way to lower the number of infected individuals and reduce pathogenic bacteria.

Cheneke and Ayinde (2022) created a fractional-order SIRB cholera model. They showed that combining vaccination, hygiene, and water chlorination is the most effective and cost-efficient way to control the disease. Baba et al. (2022) developed a nonlinear fractional SVIR-B model to consider imperfect vaccination and treatment in countries with cholera. This model shows positivity and boundedness and looks at optimal control problems involving vaccination, media coverage, treatment, and sanitation. Alsammani et al. (2025) developed a detailed model for Vibrio cholerae transmission. It combines human, environmental, and vaccination strategies. Numerical simulations show significant drops in infection rates and shorter epidemic durations. Treating water is essential for effective prevention.

Maity et al. (2025) created a compartment-based cholera model that includes phytoplankton-zooplankton

interactions. They found that transmission mediated by zooplankton can lead to unexpected results. Saad et al. (2025) developed a cholera model that looks at water-borne and horizontal transmissions, the infectivity of deceased individuals, and the complex relationship between vaccination strategies and disease dynamics. Al-Shafari et al. (2024) created a compartmental model to study how cholera and malaria co-infect. They found that malaria increases susceptibility to cholera, but cholera does not significantly affect malaria risk. They reviewed seven control strategies, including vector control, water sanitation, and treatment, concluding that vector control is the most cost-effective method.

Momoh et al. (2025) developed an optimal control model for the dynamics of malaria and cholera co-infection. This model focuses on five key interventions: treated bed nets, malaria treatment, and indoor residual spraying, sanitation, and cholera treatment. They developed a nonlinear system of differential equations, identified key parameters, and tackled an optimal control problem using Pontryagin's Maximum Principle. Simulation results showed how effective these interventions were in reducing the disease burden. The model builds on previous work by including bacterial shedding from both symptomatic and asymptomatic individuals and a dynamic environmental reservoir. The paper is organized as follows: the introduction in section 1, model formulation in section 2, basic properties of the model in section 3, basic reproduction number in section 4, section 5, "Equilibrium points," section 6, "Sensitivity analysis," section 7, "Optimal control formulation," and section 8, "Discussion."

2. Methodology

2.1 Model formulation

A deterministic compartmental model describes the transmission dynamics of cholera, considering the environmental transmission route. The total population is divided into seven compartments: $S(t)$: susceptible individuals, $V(t)$: vaccinated individuals, $I_S(t)$: symptomatic infected individuals, $I_A(t)$: asymptomatic infected individuals, $Q(t)$: quarantined individuals, $R(t)$: recovered individuals, and $B(t)$: environmental concentration of Vibrio cholerae. Individual are recruited into the susceptible population at a rate Λ, all the compartment experience natural death (at a rate, μ), while susceptible are vaccinated at a rate ϕ and experience a waning immunity at a rate ε and progression to infection after exposure to contaminated water. The force of infection is modeled using a nonlinear saturated incidence function: $\lambda = {\beta B}/{K+B}$, where β is the maximum ingestion rate of contaminated water and K is the half-saturation constant. Vaccine imperfection is represented by the parameter $(1-\delta)$ with δ indicating vaccine effectiveness. After infection, individuals transition to symptomatic or asymptomatic states with probabilities ω and $(1-\omega)$, respectively. The transition rates at which asymptomatic develop symptoms is γ, and symptomatic individual are quarantine at a rate σ. The recovery rates for quarantine, symptomatic, and asymptomatic

are: α, ρ and γ_1. The shedding rates for symptomatic and asymptomatic individuals are θ_1 and θ_2; and δ_1, δ_2 are the death rates caused by the disease. ω and κ are the rates at which susceptible and vaccinated individuals become symptomatic. δ_0, is the natural induced death rate of the pathogen. τ is the rate at which recovered individual become susceptible again. The governing system of the model is given by:

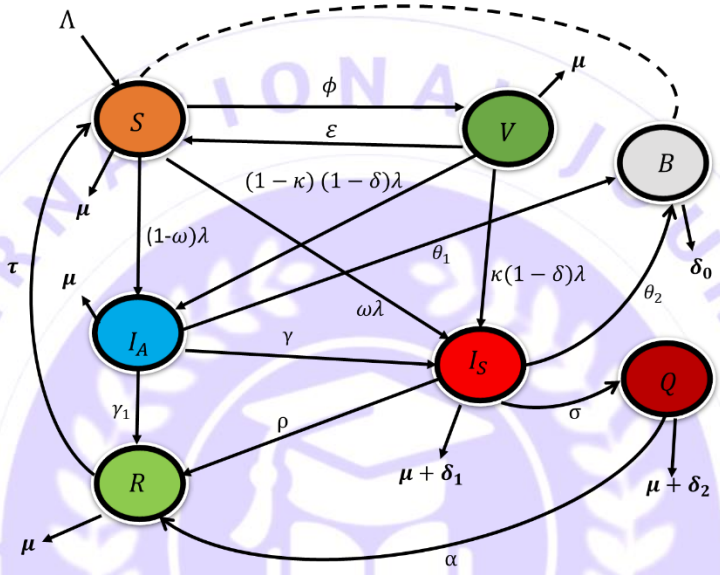

Figure 1. Schematic Diagram of the cholera model

$$\left.\begin{aligned}
\frac{dS}{dt} &= \Lambda + \varepsilon V + \tau R - (\mu + \lambda + \phi) S \\
\frac{dV}{dt} &= \phi S_H - (\mu + (1-\delta)\lambda + \varepsilon) V \\
\frac{dI_A}{dt} &= (1-\omega)\lambda S + (1-\kappa)(1-\delta)\lambda V - (\mu + \gamma + \gamma_1) I_A \\
\frac{dI_S}{dt} &= \omega\lambda S + \kappa(1-\delta)\lambda V + \gamma I_A - (\mu + \delta_1 + \rho + \sigma) I_S \\
\frac{dQ}{dt} &= \sigma I_S - (\mu + \delta_2 + \alpha) Q \\
\frac{dR}{dt} &= \gamma_1 I_A + \rho I_S + \alpha Q - (\mu + \tau) T \\
\frac{dB}{dt} &= \theta_2 I_A + \theta_1 I_S - \delta_0 B
\end{aligned}\right\} \quad (1.1)$$

Table 1. Model Parameter Description

Parameter	Description
Λ	Recruitment Rate
μ	Natural Death Rate
ϕ	Vaccination Rate
ε	Loss of Vaccine Immunity Rate
τ	Natural Loss of Recovery Immunity Rate
ω	Fraction of Infections that Become Symptomatic
γ_1, ρ	Recovery Rates for Asymptomatic and Symptomatic Individuals
δ_1, δ_2	Disease-Induced Death Rates for Infectious and Quarantined Individuals
κ	Fraction of Vaccinated that Becomes Symptomatic
α	Recovery Rate from Quarantine
θ_1, θ_2	Bacterial Shedding Rates
δ_0	Bacterial Decay Rate
K	Half-saturated constant

3. Basic Properties of the Model

3.1 Positivity of the Solution

Theorem 1: Suppose that the initial data for the model (1.1) be $S(0)>0,\ V(0)>0,\ I_A(0)\geq 0,\ I_S(0)\geq 0,\ Q(0)\geq 0, R(0)\geq 0,\ B(0)\geq 0$, then the solution $S(t),\ V(t),\ I_A(t), I_S(t), Q(t), R(t)$ and $B(t)$ of the model (1.1) with positive initial data will remain positive for all $t>0$.

Proof.

Let $t_1 = \sup\{t>0 : S(0)>0, V(0)>0, I_A(0)\geq 0, I_S(0)\geq 0, Q(0)\geq 0, R(0)\geq 0, B(0)\geq 0\} > 0$ and from the first equation of the model 1, we have

$$\frac{dS}{dt} + (\mu + \lambda + \phi)S = \Lambda + \varepsilon V + \tau R > 0. \tag{1.2}$$

Whose solution is,

$$S(t_1) = S(0)\exp\left(-(\mu+\phi)t_1 - \int_0^{t_1}\lambda(x)dx\right) + \left\{\exp\left(-(\mu+\phi)t_1 - \int_0^{t_1}\lambda(x)dx\right)\right\}$$

$$\int_0^{t_1}(\Lambda + \varepsilon V + \tau R)\exp\left(-(\mu+\phi)t_1 - \int_0^{t_1}\lambda(x)dx\right)dz > 0.$$

Hence similarly it can be shown that

$V(t)>0, I_A(t)\geq 0, I_S(t)\geq 0, Q(t)\geq 0, R(t)\geq 0$ and $B(t)\geq 0$ for all $t>0$. Hence all the solutions of the model remain positive for all $t>0$. Hence, all solutions of the model (1.1) remain non-negative.

3.2 The Invariant Region

Theorem 2: The closed set

$$\Pi = \Pi_H \bigcup \Pi_B \subseteq \mathbb{R}_+^6 \times \mathbb{R}_+ \tag{1.3}$$

where,

$$\Pi_H = \left\{ (S, V, I_A, I_S, Q, R) \in \mathbb{R}_+^6 ; N_H \leq \frac{\Lambda}{\mu} \right\} \text{ and}$$

$$\Pi_B = \left\{ B \in \mathbb{R}_+ ; B \leq \frac{\Lambda(\theta_1 + \theta_2)}{\mu \delta_0} \right\} \tag{1.4}$$

is positively- invariant and attract all the positive solutions of the model.

Proof

Adding equations in system, yield

$$\frac{dN_H}{dt} \leq \Lambda - \mu N_H \tag{1.5}$$

By comparison theorem (Lakshmikantham *et al*., 2015), we have

$$N_H(t) \leq N_H(0) e^{-\mu t} + \frac{\Lambda}{\mu}\left(1 - e^{-\mu t}\right), \text{ for all } t \geq 0 . \tag{1.6}$$

Similarly for the pathogen class, we have

$$\dot{B}(t) = \theta_2 I_A + \theta_1 I_S - \delta_0 B \leq (\theta_2 + \theta_1) N_H - \delta_0 B \leq \frac{(\theta_2 + \theta_1)\Lambda}{\mu} - \delta_0 B . \tag{1.7}$$

Again by comparison theorem, we have

$$B(t) \leq B(0) e^{-\delta_0 t} + \frac{(\theta_2 + \theta_1)\Lambda}{\mu}\left[1 - e^{-\delta_0 t}\right] . \tag{1.8}$$

At $t \to \infty$ the inequality becomes $N_H \leq \frac{\Lambda}{\mu}$, which shows that the feasible solution of the system as $N_H \to \frac{\Lambda}{\mu}$ is the system consist of five possible solutions and the solution model for this system is uniformly bounded in the subset of $\mathbb{R}_+^6$ the feasible solution of the region Π_H is positively invariant and attracting with respect to system Π_H . Similarly, $B(t) \to \frac{(\theta_2 + \theta_1)\Lambda}{\mu}$, hence Π, is positively invariant.

2.3 Basic reproduction number

The reproduction number $\mathcal{R}_0$ is defined as the average number of secondary cases of infection generated by one primary case in a whole susceptible population. The method of the next generation on the system 1.1 was adopted (Van den Driessche and Warmouth, 2002). Following the approach in Sanda *el al,* 2024, we obtained the matrices F and V for the new infection terms and the remaining transfer terms are, respectively,

$$F=\begin{bmatrix} 0 & 0 & \frac{\beta}{K}\left[(1-\kappa)(1-\delta)V^{*}+(1-\omega)S^{*}\right] \\ 0 & 0 & \frac{\beta}{K}\left[\kappa(1-\delta)V^{*}+\omega S^{*}\right] \\ 0 & 0 & 0 \end{bmatrix} \text{ and } V=\begin{bmatrix} h_3 & 0 & 0 \\ -\gamma & h_4 & 0 \\ -\theta_2 & -\theta_1 & \delta_0 \end{bmatrix}$$

Hence,

$$\mathcal{R}_0=\frac{\beta\Lambda}{K\delta_0\mu h_3 h_4(\mu+\varepsilon+\phi)}\left\{\left((1-\kappa)(1-\delta)\phi+h_2(1-\omega)\right)(\theta_2 h_4+\theta_1\gamma)+\theta_1 h_3\left(\kappa(1-\delta)\phi+h_2\omega\right)\right\}$$

2.4 Equilibrium points

Setting the RHS of system (1.1) to zero and at DFE $(\mathcal{E}_0)$ $B=I_A=I_S=0$, we obtained

$$\mathcal{E}_0=\left\{S^{*},V^{*},I_A^{*},I_S^{*},Q^{*},R^{*},B^{*}\right\}=\left\{\frac{\Lambda(\mu+\varepsilon)}{\mu(\varepsilon+\mu+\phi)},\frac{\Lambda\phi}{\mu(\varepsilon+\mu+\phi)},0,0,0,0,0\right\} \quad (1.9)$$ and

the endemic equilibrium point $\mathcal{E}_1=\left\{S^{**},V^{**},I_A^{**},I_S^{**},Q^{**},R^{**},B^{**}\right\}$ by also setting the RHS of the system 1.1 to zero, then $S^{**}=\frac{\Lambda+\varepsilon V^{**}+\tau R^{**}}{h_1+\lambda^{**}}$, $V^{**}=\frac{\phi S^{**}}{h_2+(1-\delta)\lambda^{**}}$, $I_A^{**}=\frac{\left[(1-\omega)S^{**}+(1-\kappa)(1-\delta)V^{**}\right]\lambda^{**}}{h_3}$,

$I_S^{**}=\frac{\left[\omega S^{**}+\kappa(1-\delta)V^{**}\right]\lambda^{**}}{h_4}$, $Q^{**}=\frac{\phi I_S^{**}}{h_5}$, $R^{**}=\frac{\gamma_1 I_A^{**}+\rho I_S^{**}+\alpha Q^{**}}{h_6}$, $B^{**}=\frac{\theta_2 I_A^{**}+\theta_1 I_S^{**}}{\delta_0}$ Let,

$$\begin{aligned} &h_1=(\mu+\lambda+\phi),\ h_2=(\mu+\varepsilon),\ h_3=(\mu+\gamma+\gamma_1),h_4=(\mu+\delta_1+\rho+\sigma),\\ &h_5=(\mu+\delta_2+\alpha),\ h_6=(\mu+\tau). \end{aligned} \quad (1.10)$$

Now evaluating $\lambda^{**}=\frac{\beta B^{**}}{K+B^{**}}$, EEP, yield

$$\Delta_1\lambda^{**^2}+\Delta_2\lambda^{**}+\Delta_3=0 \quad (1.11)$$

where, $\Delta_1=K\delta_0(1-\delta)h_3h_4h_5h_6-K\delta_0h_{12}+\beta\pi h_{14}h_5h_6$,

$\Delta_2=K\delta_0h_3h_4h_5h_6\left((1-\delta)h_1+h_2\right)-K\delta_0h_{11}$ $\Delta_3=\mu K\delta_0h_3h_4h_5h_6(\varepsilon+\mu+\phi)(1-\mathcal{R}_0)$

$h_8=(1-\omega)h_2+(1-\kappa)(1-\delta)\phi,\ h_9=\omega h_2h_3+\kappa(1-\delta)h_3+\gamma h_8$

$h_{10}=\omega(1-\delta)h_3+\gamma(1-\delta)(1-\omega)h_3, h_{11}=\gamma h_4h_5h_8+\rho h_5h_9+\alpha\rho\sigma h_9,$ Therefore the

$h_{12}=\gamma_1h_4h_5(1-\omega)(1-\delta)+\rho h_5h_{10}+\alpha\rho\sigma h_{10},\ h_{13}=\theta_2h_4h_8+\theta_1h_9,$

$h_{13}=\theta_2h_4(1-\omega)(1-\delta)+\theta_1h_{10}$

endemic equilibrium point exist and is unique when $\mathcal{R}_0 > 1$, by Descarte rule of sign.

Theorem 3: The disease free equilibrium $\mathcal{E}_0$, of the cholera model 1.1 is globally asymptotically stable if $\mathcal{R}_0 < 1$ and unstable if otherwise.

Proof

To prove the global stability of the disease-free equilibrium (DFE) for the model (1.1), we use the method of Lyapunov functions. Consider the function

$$\mathcal{L} = p_1 I_A + p_2 I_S + p_3 B, \tag{1.12}$$

whose derivative is given as

$$\frac{d\mathcal{L}}{dt} = p_1 \frac{dI_A}{dt} + p_2 \frac{dI_S}{dt} + p_3 \frac{dB}{dt}. \tag{1.13}$$

Substituting $\dot{I}_A$, $\dot{I}_S$ and $\dot{B}$ in (1.13), we have

$$\begin{aligned} \frac{d\mathcal{L}}{dt} &= p_1\left((1-\omega)\lambda S + (1-\kappa)(1-\delta)\lambda V - (\mu+\gamma+\gamma_1) I_A\right) \\ &+ p_2\left(\omega\lambda S + \kappa(1-\delta)\lambda V + \gamma I_A - (\mu+\delta_1+\rho+\sigma) I_S\right) + p_3\left(\theta_2 I_A + \theta_1 I_S - \delta_0 B\right) \end{aligned} \tag{1.14}$$

$$\begin{aligned} \frac{d\mathcal{L}}{dt} &= \left[p_1(1-\omega) + p_2\omega\right]\lambda S + \left[p_1(1-\kappa)(1-\delta) + p_2\kappa(1-\delta)\right]\lambda V \\ &+ \left[p_2\gamma + p_3\theta_2 - p_1 h_3\right] I_A + \left[p_3\theta_1 - p_2 h_4\right] I_S - p_3\delta_0 B \end{aligned}$$

At the DFE, $S \le S^*$ and $V \le V^*$. Also $\lambda = \frac{\beta B}{K+B} \le \frac{\beta}{K} B$ (since $K + B \ge K$).

Then

$$\begin{aligned} \frac{d\mathcal{L}}{dt} &\le \left[p_1(1-\omega) + p_2\omega\right]\frac{\beta}{K} B S^* + \left[p_1(1-\kappa)(1-\delta) + p_2\kappa(1-\delta)\right]\frac{\beta}{K} B V^* \\ &+ \left[p_2\gamma + p_3\theta_2 - p_1 h_3\right] I_A + \left[p_3\theta_1 - p_2 h_4\right] I_S - p_3\delta_0 B \end{aligned} \tag{1.15}$$

Let $\Upsilon = \frac{\beta}{K}\left\{\left[p_1(1-\omega) + p_2\omega\right] S^* + \left[p_1(1-\kappa)(1-\delta) + p_2\kappa(1-\delta)\right] V^*\right\} - p_3\delta_0$

Then,

$$\frac{d\mathcal{L}}{dt} \le \Upsilon B + \left[p_2\gamma + p_3\theta_2 - p_1 h_3\right] I_A + \left[p_3\theta_1 - p_2 h_4\right] I_S \tag{1.16}$$

Evaluating p_1, p_2, p_3, we have, $p_1 = \frac{\theta_1}{h_4}$, $p_2 = \frac{1}{h_3}\left(\frac{\theta_1\gamma}{h_4} + \theta_2\right)$, $p_3 = 1$ (1.17)

Substituting yield in Υ

$$\Upsilon = \frac{\beta}{K}\left\{\left[\frac{\theta_1}{h_4}(1-\omega)+\frac{1}{h_3}\left(\frac{\theta_1\gamma}{h_4}+\theta_2\right)\omega\right]S^*+\left[\frac{\theta_1}{h_4}(1-\kappa)(1-\delta)+\frac{1}{h_3}\left(\frac{\theta_1\gamma}{h_4}+\theta_2\right)\kappa(1-\delta)\right]V^*\right\}-\delta_0$$

$$=\frac{\beta}{K}\left\{\frac{1}{h_3}\left(\frac{\theta_1\gamma}{h_4}+\theta_2\right)\left(\omega S^*+\kappa(1-\delta)V^*\right)+\frac{\theta_1}{h_4}\left((1-\omega)S^*+(1-\kappa)(1-\delta)V^*\right)\right\}-\delta_0$$

$$=\delta_0\left(\frac{\beta}{K\delta_0}\left\{\frac{1}{h_3}\left(\frac{\theta_1\gamma}{h_4}+\theta_2\right)\left(\omega S^*+\kappa(1-\delta)V^*\right)+\frac{\theta_1}{h_4}\left((1-\omega)S^*+(1-\kappa)(1-\delta)V^*\right)\right\}-1\right)$$

Thus,
$$\frac{d\mathcal{L}}{dt} \le \Upsilon B \le \delta_0\left[\mathcal{R}_0-1\right]B. \tag{1.18}$$

Therefore $B \ge 0$ if and only if $\mathcal{R}_0 < 1$, $\dot{\mathcal{L}} < 0$. Since all the parameters are non-negative it follows that $\dot{\mathcal{L}} = 0$ if and only if $B = 0$. Hence $\mathcal{L}$ is a Lyapunov function on Π. Therefore by LaSalle's Invariant Principles (LaSalle and Lefschetz, 1961) every solution to the model with initial condition in Π, approaches $\mathcal{E}_0$ as $t \to \infty$ whenever $\mathcal{R}_0 < 1$ so that $\mathcal{E}_0$ is GAS in Π. The biological implication of the above result is that it rules out the existence of backward bifurcation which implies that $\mathcal{R}_0 < 1$ is sufficient for the cholera model to die out from the population (as seen in Figure 2).

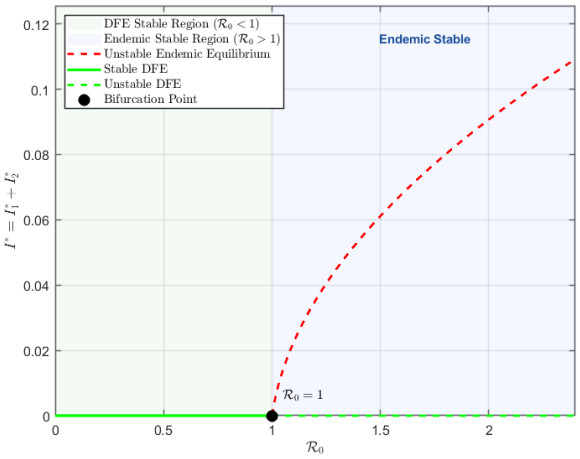

Figure 2. Forward Bifurcation Diagram with Stability Regions

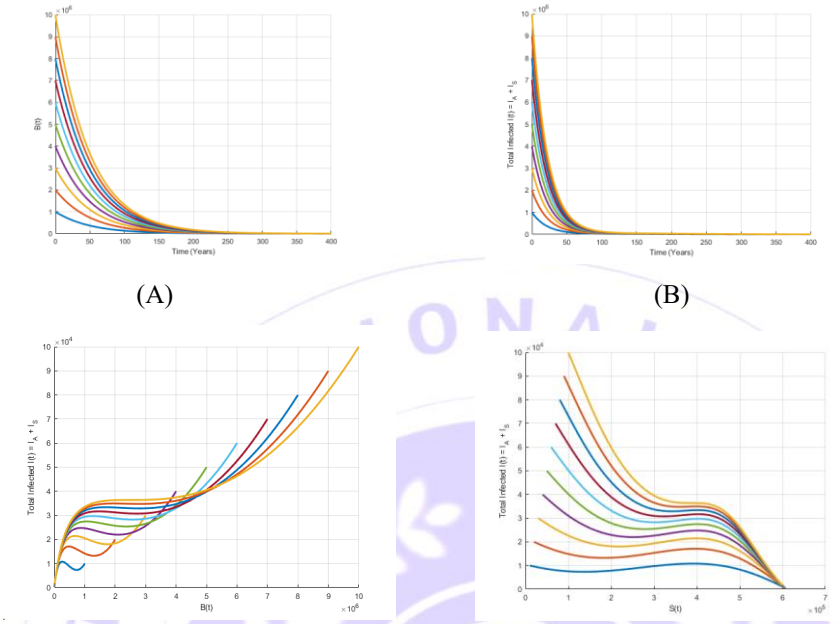

(A) (B)

(C) (D)

Figure 3. Simulation showing the convergence to $\mathcal{E}_0$, when $\mathcal{R}_0 < 1$.

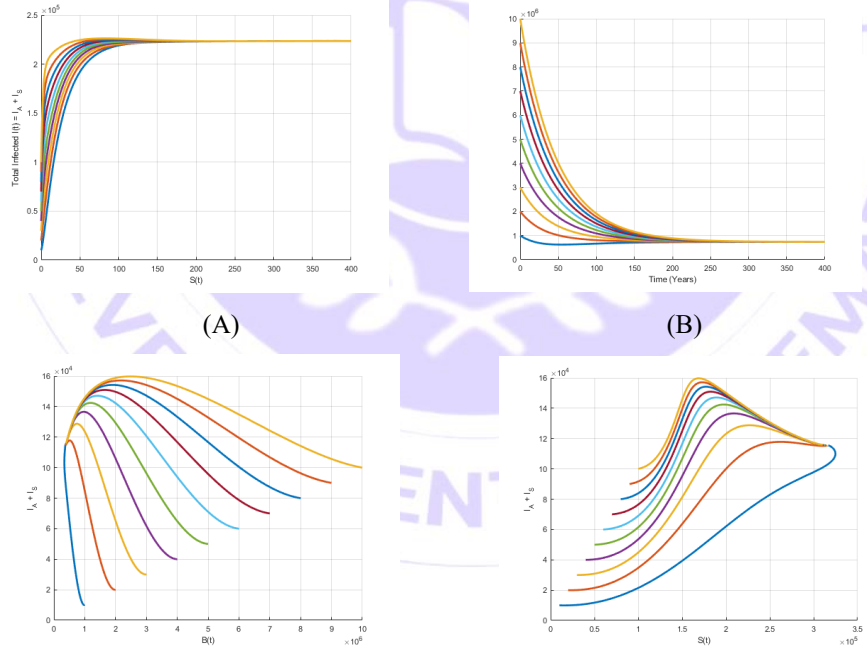

(A) (B)

(C) (D)

Figure 4. Simulation showing the convergence to $\mathcal{E}_1$, when $\mathcal{R}_0 > 1$.

6.0 Sensitivity Analysis

A sensitivity analysis was performed to determine the relative impact of model parameters on the basic reproduction number, $\mathcal{R}_0$, for the cholera transmission model. The results of the normalized sensitivity analysis are presented in Figure 4, which shows β, the maximum ingestion rate of contaminated water and Λ the recruitment rate of susceptible individuals) both exhibit the highest positive sensitivity indices, each with an elasticity of approximately +1. These parameters with the highest magnitude of sensitivity indices exert the greatest influence on disease transmission dynamics and indicates that a proportional increase in either of these parameters leads to a proportional increase in $\mathcal{R}_0$. Thus, higher ingestion of contaminated water or increased entry of susceptible into the population promotes disease spread. Conversely, the natural death rate μ and vaccination rate ϕ display the strongest negative sensitivities, each with an elasticity of approximately –1. These results imply that increasing either μ or ϕ substantially reduces $\mathcal{R}_0$, reflecting the critical roles of mortality and vaccination in curtailing cholera transmission. Moderate positive sensitivities were observed for the waning immunity rate ε, which suggests that faster loss of immunity increases $\mathcal{R}_0$. Similarly, parameters associated with bacterial shedding rates (θ_1, θ_2) and the probability of developing symptomatic infection (ω) exhibited smaller positive sensitivities, indicating that higher shedding or symptomatic proportions increase the level of environmental contamination and, consequently, transmission potential. On the other hand, recovery-related parameters (α, ρ, γ_1) demonstrated negative sensitivities, signifying that enhanced recovery from infection or quarantine effectively reduces $\mathcal{R}_0$. Parameters related to vaccine effectiveness (δ) and the pathogen decay rate in the environment (δ_0) also contributed negatively but with lesser magnitudes.

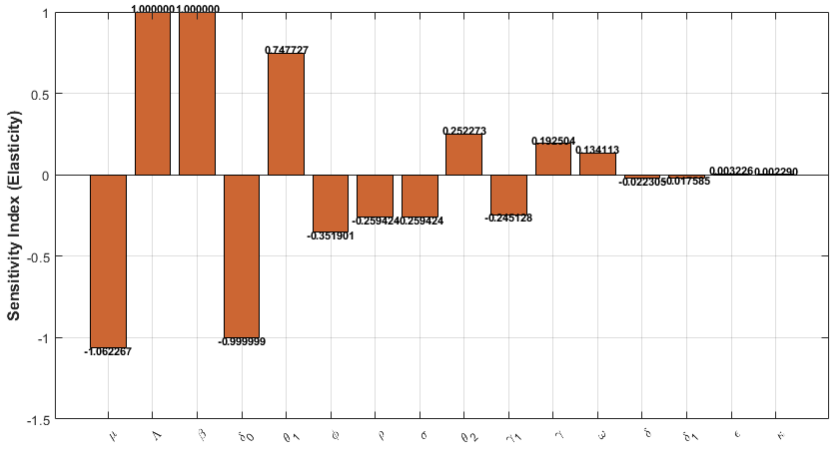

Figure 5. Sensitivity analysis of the $\mathcal{R}_0$ showing the influence of the parameters.

3. Optimal Control Formulation

The goal is to minimize infection and environmental bacterial concentration while reducing control implementation costs. We assume that the control functions, $u_1(t)$, $u_2(t)$ and $u_3(t)$ are bounded, Lebesgue integrable functions, where the control $u_1(t)$ is the public awareness/education control, $u_2(t)$ is the quarantine control and $u_3(t)$ accounts for treatment of infected population.

$$\left.\begin{aligned}
\frac{dS}{dt} &= \Pi + \varepsilon V + \tau R - \left(\mu + (1-u_1)\lambda + \phi\right)S \\
\frac{dV}{dt} &= \phi S_H - \left(\mu + (1-\delta)(1-u_1)\lambda + \varepsilon\right)V \\
\frac{dI_A}{dt} &= (1-\omega)(1-u_1)\lambda S + (1-\kappa)(1-\delta)(1-u_1)\lambda V - (\mu+\gamma+\gamma_1+u_3)I_A \\
\frac{dI_S}{dt} &= \omega\lambda S + \kappa(1-\delta)(1-u_1)\lambda V + \gamma I_A - (\mu+\delta_1+\rho+\sigma u_2+u_3)I_S \\
\frac{dQ}{dt} &= u_2\sigma I_S - (\mu+\delta_2+\alpha+u_3)Q \\
\frac{dR}{dt} &= \gamma_1 I_A + \rho I_S + \alpha Q + u_3(I_A+I_S+Q) - (\mu+\tau)T \\
\frac{dB}{dt} &= (1-u_1)(\theta_2 I_A + \theta_1 I_S) - (\delta_0+u_1)B
\end{aligned}\right\}$$

The objective functional to be minimized is

$$J\left[u_1(t), u_2(t), u_3(t)\right] = \min \int_0^{t_f} \left[b_1 I_A + b_2 I_S + b_3 B + \frac{1}{2}\left(a_1 u_1^2 + a_2 u_2^2 + a_3 u_3^2\right)\right] dt. \qquad (1.21)$$

The associated relevant cost is made of the cost for effective treatment and the cost for vaccination of the susceptible population. Here we assume that the cost associated with objective functional is nonlinear with the quadratic form (Lenhart & Workman, 2007). Where b_i, $(i=1,2,3)$ are weight constant associated with the cost of minimizing the I_A, I_S and B populations respectively and a_i, $(i=1,2,3)$ are the weight constants for control effects respectively. Thus, the cost of public awareness the susceptible population is $\frac{a_1 u_1^2}{2}$, while the cost of quarantine is $\frac{a_2 u_2^2}{2}$ and the cost of proper treatment is $\frac{a_3 u_3^2}{2}$. Let $u = (u_1, u_2, u_3)$ be a control on system (1.1) and a set of admissible

$$\Pi = \left\{ u_1, u_2, u_3 \in L^1(0, t_f) / u \in \mathrm{M}^3, \mathrm{M} = [0,1], \forall t \in [0, t_f] \right\}. \qquad (1.22)$$

Therefore, we want to find an optimal control $u^* = (u_1^*, u_2^*, u_3^*)$ such that

$$J\left(u^*\right)=\min_{\Omega_T} J\left(u\right) \tag{1.23}$$

The necessary condition that an optimal pair must satisfy comes from the Pontryagen's maximum principles. This principle converts the system (1.1) into a problem of minimizing point wise and Hamilton *H,* with respect t u_1,u_2,u_3 S,V,I_A,I_S,Q,R,B

$$\begin{aligned}
H &= b_1I_A+b_2I_S+b_3B+\frac{1}{2}a_1u_1^2\frac{1}{2}a_2u_2^2+\frac{1}{2}a_3u_3^2\\
&+\xi_1\left\{\Pi+\varepsilon V+\tau R-\left(\mu+\left(1-u_1\right)\lambda+\phi\right)S\right\}\\
&+\xi_2\left\{\phi S_H-\left(\mu+\left(1-\delta\right)\left(1-u_1\right)\lambda+\varepsilon\right)V\right\}\\
&+\xi_3\left\{\left(1-\omega\right)\left(1-u_1\right)\lambda S+\left(1-\kappa\right)\left(1-\delta\right)\left(1-u_1\right)\lambda V-\left(\mu+\gamma+\gamma_1+u_3\right)I_A\right\}\\
&+\xi_4\left\{\omega\lambda S+\kappa\left(1-\delta\right)\left(1-u_1\right)\lambda V+\gamma I_A-\left(\mu+\delta_1+\rho+\sigma u_2+u_3\right)I_S\right\}\\
&+\xi_5\left\{u_2\sigma I_S-\left(\mu+\delta_2+\alpha+u_3\right)Q\right\}\\
&+\xi_6\left\{\gamma_1I_A+\rho I_S+\alpha Q+u_3\left(I_A+I_S+Q\right)-\left(\mu+\tau\right)R\right\}\\
&+\xi_7\left\{\left(1-u_1\right)\left(\theta_2I_A+\theta_1I_S\right)-\left(\delta_0+u_1\right)B\right\}
\end{aligned}$$

Theorem 2. The optimal control $u_i\left(i=1,2,3\right)$ and the solutions S_H,V,I_A,I_S,Q,R,B of the model (1.1) that minimize $J\left(u_1,u_2,u_3\right)$ over Π. Furthermore, there exist ad joint function $\xi_i\left(i=1,2,...,7\right)$ such that

$$\begin{cases}
\frac{d\xi_1}{dt}=\phi\left(\xi_1-\xi_2\right)+\left(1-u_1\right)\omega\lambda\left(\xi_1-\xi_4\right)+\left(1-u_1\right)\left(1-\omega\right)\lambda\left(\xi_1-\xi_3\right)+\mu\xi_1\\
\frac{d\xi_2}{dt}=\varepsilon\left(\xi_2-\xi_1\right)+\kappa\left(1-\delta\right)\left(1-u_1\right)\lambda\left(\xi_2-\xi_4\right)+\left(1-\kappa\right)\left(1-\delta\right)\left(1-u_1\right)\left(\xi_2-\xi_3\right)+\mu\xi_2\\
\frac{d\xi_3}{dt}=\gamma\left(\xi_3-\xi_4\right)+\left(\gamma_1+u_3\right)\left(\xi_3-\xi_6\right)+\mu\xi_2+b_1\\
\frac{d\xi_4}{dt}=\sigma u_2\left(\xi_4-\xi_5\right)+\left(\rho+u_3\right)\left(\xi_4-\xi_6\right)+\left(\mu+\delta_1\right)\xi_4+b_2\\
\frac{d\xi_5}{dt}=\left(\alpha+u_3\right)\left(\xi_4-\xi_6\right)+\left(\mu+\delta_2\right)\xi_5\\
\frac{d\xi_6}{dt}=\tau\left(\xi_6-\xi_1\right)+\mu\xi_6\\
\frac{d\xi_7}{dt}=\left(1-u_1\right)\frac{\beta K\omega S}{\left(K+B\right)^2}\left(\xi_1-\xi_4\right)+\left(1-u_1\right)\frac{\beta K\left(1-\omega\right)S}{\left(K+B\right)^2}\left(\xi_1-\xi_3\right)+\mu\xi_1\\
\left(1-u_1\right)\frac{\beta K\kappa\left(1-\delta\right)V}{\left(K+B\right)^2}\left(\xi_2-\xi_4\right)+\left(1-u_1\right)\frac{\beta K\left(1-\kappa\right)\left(1-\delta\right)V}{\left(K+B\right)^2}\left(\xi_2-\xi_3\right)\\
+\xi_7\left(u_1+\delta_0\right)+b_3
\end{cases} \tag{4.121}$$

With transversity conditions.

$$\xi_i\left(t_f\right)=0, \qquad i=1,2,...,7 \tag{4.122}$$

The optimality conditions for the model are

$$H\left(S,V,I_A,I_S,Q,R,B,\lambda_i\right)=\min_{0\le u_1,u_2,u_3\le 1} H\left(S,V,I_A,I_S,Q,R,B,u_i,\xi_i\right)$$

with optimal control characterized as

$$\begin{cases} u_1^*(t)=\min\left\{\max\left\{\frac{1}{a_1}\begin{pmatrix}\lambda\omega S\left(\xi_4-\xi_1\right)+\lambda\left(1-\omega\right)S\left(\xi_3-\xi_1\right)+\lambda\kappa\left(1-\delta\right)V\left(\xi_3-\xi_2\right)\\ +\lambda\left(1-\kappa\right)\left(1-\delta\right)V\left(\xi_4-\xi_2\right)+\left(\theta_2 I_A+\theta_1 I_S\right)\xi_7\end{pmatrix}\right\},1\right\} \\ u_2^*(t)=\min\left\{\max\left\{\frac{1}{a_2}\left(\sigma I_S\left(\lambda_4-\lambda_5\right)\right)\right\},1\right\} \\ u_3^*(t)=\min\left\{\max\left\{\frac{1}{a_3}\left\{I_S\left(\xi_4-\xi_6\right)+I_A\left(\xi_3-\xi_6\right)+B\left(\xi_5-\xi_6\right)\right\}\right\},1\right\} \end{cases} \tag{4.123}$$

Proof

Consider the Hamiltonian function, the adjoint equations are obtained by differentiating the Hamiltonian function *H* partially and evaluated at the controls. Thus, by Pontryagen's maximum principle, we obtained

$$\frac{d\xi_1}{dt}=-\frac{\partial H}{\partial S},\frac{d\xi_2}{dt}=-\frac{\partial H}{\partial V},\frac{d\xi_3}{dt}=-\frac{\partial H}{\partial I_A},\frac{d\xi_4}{dt}=-\frac{\partial H}{\partial I_S},\frac{d\xi_5}{dt}=-\frac{\partial H}{\partial Q},\frac{d\xi_6}{dt}=-\frac{\partial H}{\partial R},\frac{d\xi_7}{dt}=-\frac{\partial H}{\partial B}.$$

With zero final time condition (transversely)

$$\xi_i\left(t_f\right)=0, \qquad i=1,2,...,7.$$

and the characteristics of the fractional optimal control is obtained by solving the equations

$$\frac{\partial H}{\partial u_1}=0,\ \frac{\partial H}{\partial u_2}=0 \ \text{ and } \ \frac{\partial H}{\partial u_3}=0.$$

on the interior of the control set and this concludes the proof.

Table 2: Model Parameters, Values, and Sources

Parameter	Value	Source
Λ	10000 year^{-1}	Nelson et al. (2025)
μ	0.012 year^{-1}	Mukandavire et al. (2011)
ϕ	1.7 % year^{-1}	Nelson et al. (2025)

ε	3 days	Nelson et al. (2025)
β	0.553 year^{-1}	Nelson et al. (2025)
K	10^6 cells/mL day^{-1}	Codeço (2001); Hartley et al. (2006)
δ	0.75	WHO (2022)
σ	1/7 day^{-1}	Assumed
α	1/5 day^{-1}	Nelson et al. (2025)
ρ	1/7 day^{-1}	Nelson et al. (2025)
γ_1	1/7 day^{-1}	Assumed
θ_1	50 day^{-1}	Nyabadza et al (2019)
θ_2	10 day^{-1}	Assumed
δ_1	0.0013 year^{-1}	Nelson et al. (2025)
δ_2	0.00013 year^{-1}	Assumed
ω	0.25/dimensionless	Assumed
κ	0.4/dimensionless	Assumed
τ	0.00042 year^{-1}	Nelson et al. (2025)
δ_0	0.004 day^{-1}	Lin et al (2019)

4. Discussion

In Figure 5(A), $\mathcal{R}_0$ is shown as a function of κ. Since the relationship is positively linear, the basic reproduction number $\mathcal{R}_0$ increase in direct proportion to the increase in κ. This implies that a greater percentage of those who exhibit symptoms are more contagious, which encourages the transmission of illness among individuals. When symptomatic individuals grow more contagious (i.e., κ approaches 1), they contribute more to environmental contamination and person-to-person transmission, increasing the overall infection potential. Conversely, lowering κ lowers $\mathcal{R}_0$, suggesting that symptomatic person-centered treatments can effectively reduce the transmission rate. Figure 5(B) illustrates that when the vaccination rate ϕ rises, $\mathcal{R}_0$ falls exponentially. This inverse association suggests that vaccination is a very good way to stop the spread of cholera. As ϕ increases, fewer people in the

population are susceptible, which reduces the disease's ability to spread. When vaccination rates are low, $\mathcal{R}_0$ stays high, suggesting a continuous danger of transmission. The possibility of achieving herd immunity is suggested by the quick drop in $\mathcal{R}_0$ toward unity as ϕ rises over specific thresholds. This emphasizes how crucial it is to implement long-term, extensive immunization campaigns in order to contain and maybe eradicate cholera epidemics. A contour plot of $\mathcal{R}_0$ vs γ_1 (recovery rate of asymptomatic persons) and ρ (recovery rate of symptomatic individuals) is shown in Figure 5(C). The contours show that $\mathcal{R}_0$ decreases as both recovery rates increase. This suggests that quicker recovery for both asymptomatic and symptomatic people shortens the average infectious period, which lowers the risk of cholera transmission. Low values of γ_1 and ρ show the greatest $\mathcal{R}_0$ values, which are indicative of delayed recovery and longer infectiousness. The contour map's cooler color areas show that $\mathcal{R}_0$ drops down dramatically as both γ_1 and ρ rise. The epidemic control boundary is denoted by the red contour line, which indicates a critical threshold at $\mathcal{R}_0 = 1$. Therefore, one of the most important ways to stop the spread of cholera is to improve recovery through efficient treatment and rehydration therapy. The contour of $\mathcal{R}_0$ in relation to vaccination rate (ϕ) and vaccine efficacy (δ) is depicted in Figure 5(D). The contour lines are almost vertical, suggesting that ϕ has a more pronounced effect on $\mathcal{R}_0$ within the studied range than changes in δ. $\mathcal{R}_0$ exhibits a modest decrease when ϕ increases, despite the minor color gradient. This suggests that increasing vaccination coverage reduces disease transmission more efficiently than slight improvements in vaccine efficiency alone. This implies that even with vaccines that are only modestly effective, cholera outbreaks can be considerably reduced by attaining widespread vaccination coverage.

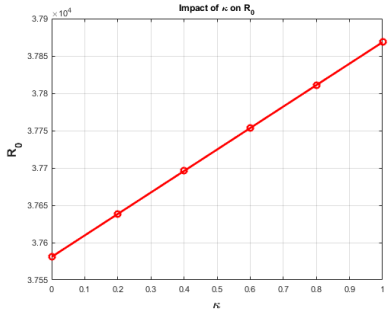

(A)

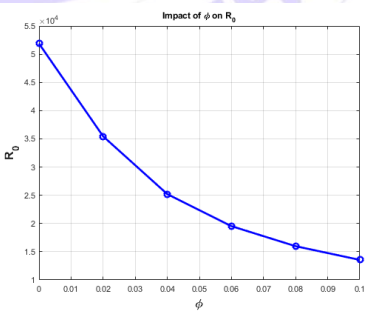

(B)

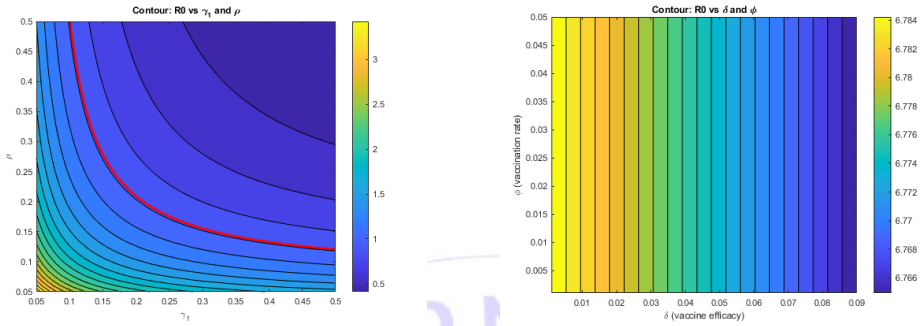

(C) (D)

Figure 6. Simulation showing (A) the impact of κ on $\mathcal{R}_0$ (B) the impact of ϕ on $\mathcal{R}_0$, (C) the contour plot of $\mathcal{R}_0$ vs ρ and γ_1 (D)) the contour plot of $\mathcal{R}_0$ vs δ and ϕ.

To assess the impact of public awareness/education, quarantine and treatment, we simulates the model with the controls and assess the impact as below.

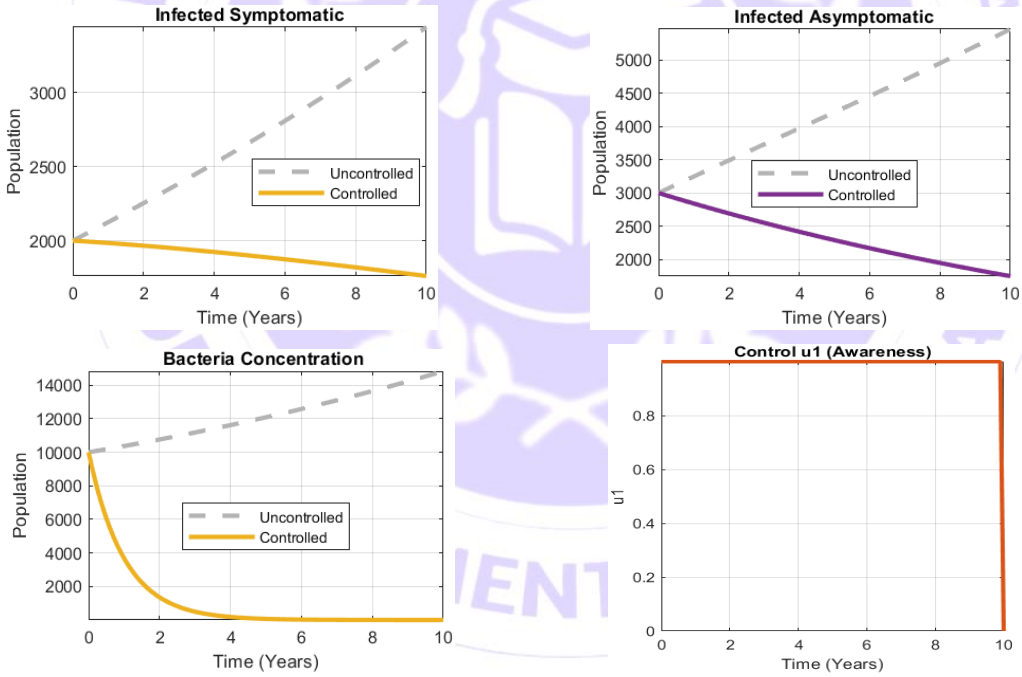

Figure 7. Numerical simulation showing impact of u_1 on the infectious and bacteria population

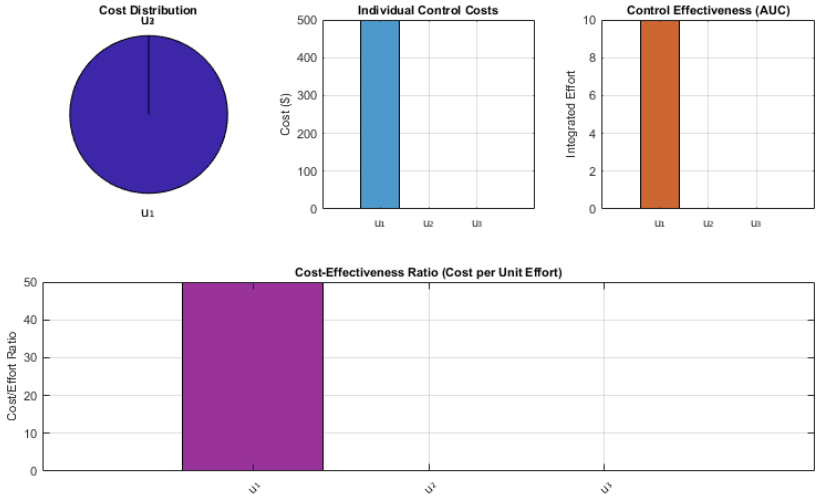

Figure 8. Numerical simulation showing the cost effectives of u_1

Figure 7 depict a decline in controlled cases, indicating successful u_1 efforts lowering new infections, and an increase in symptomatic infections in uncontrolled instances. The figure also depicts how asymptomatic infected individuals increase as a result of unidentified carriers but decreases as awareness is raised. The bacterial load in aquatic environments decreases under u_1 control, suggesting that awareness-based interventions might greatly enhance water handling and environmental cleanliness, thereby breaking the loop of transmission between humans and the environment. The plot shows that, as indicated by the control's maximum level over the course of the simulation, keeping a constant level of public awareness is essential for the best possible disease decrease. Figure 8, depicts the pie chart plot that shows that 100% of the entire cost of control is due to awareness campaigns. This means that awareness is the biggest part of the control program's budget, therefore, resources are focused on public education and communication about changing behavior. The bar chart reveals the moderate economic burden of implementing awareness, which is justifiable due to its high epidemiological impact, represented by the integral of the quadratic control term. The plot also indicates high effectiveness of awareness in reducing disease burden is evident in the Area under the curve (AUC), indicating that per unit effort, it yields substantial epidemiological benefits. The cost-effectiveness ratio (u_1) is approximately 50, indicating that the awareness intervention is cost-effective and sustainable, despite being the only control, as it reduces disease significantly relative to its cost.

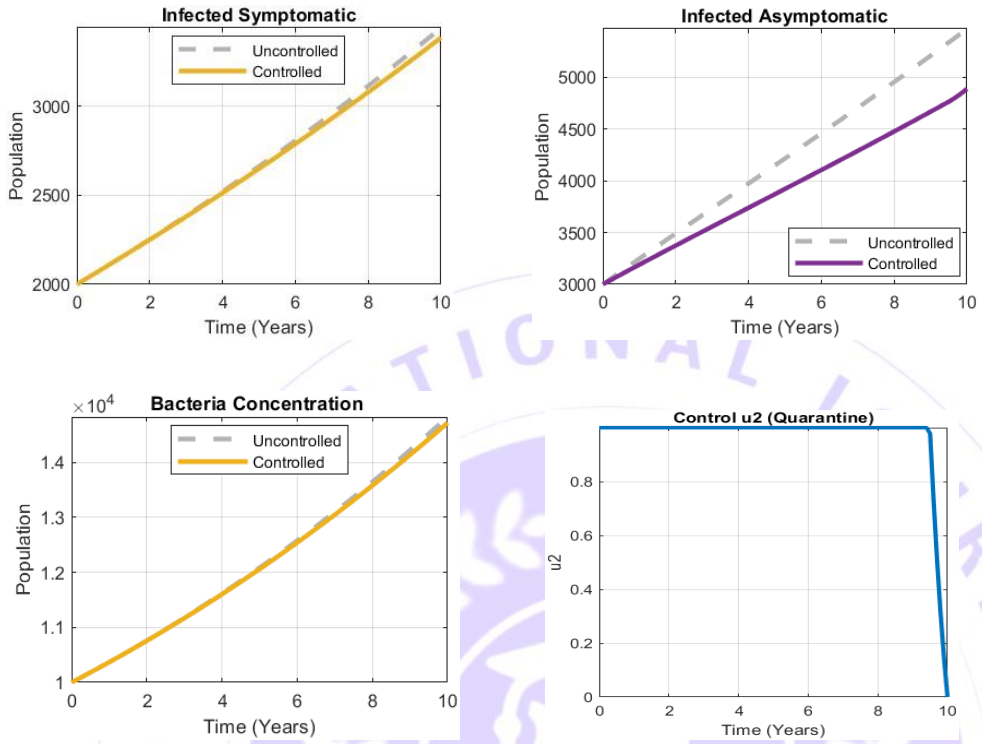

Figure 9. Numerical simulation showing impact of u_2 on the infectious and bacteria population

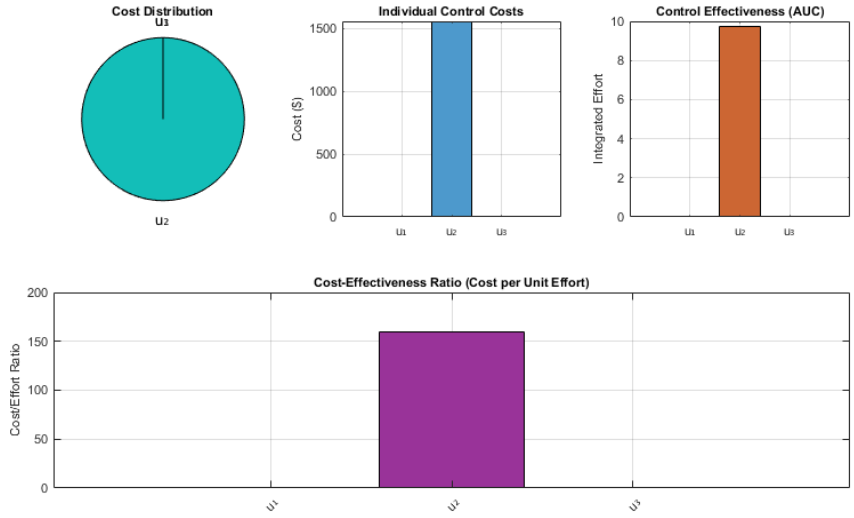

Figure 10. Numerical simulation showing the cost effectives of u_2

Figure 9 shows that the symptomatic population rises in the absence of control and falls in the presence of it. However, in the controlled scenario, u_2 causes a slight slowdown. However, u_2 (quarantine) might not be sufficient to drastically lower cases unless combined with other control measures. The figure also shows the growth rate of asymptomatic infections, with controlled cases declining over time and uncontrolled cases increasing. This implies that by restricting contact, quarantine successfully reduces transmission. Figure 10, depicts the cost distribution pie chart shows that quarantine (u_2) accounts for 100% of all control costs, indicating that all available resources are used to isolate and contain infected individuals. The bar chart shows a moderate total cost of around $1,500 for quarantine, representing the entire intervention budget in this scenario, despite being lower. The Area under the curve, (AUC) plot indicates that quarantine effectively reduces infected population and bacterial concentration, demonstrating its potential in slowing disease spread by isolating symptomatic individuals. The moderate Cost-Effectiveness Ratio (CER) value of ~160 suggests that quarantine, despite being costly, offers reasonable epidemiological benefits per dollar spent, making it an efficient single-control strategy.

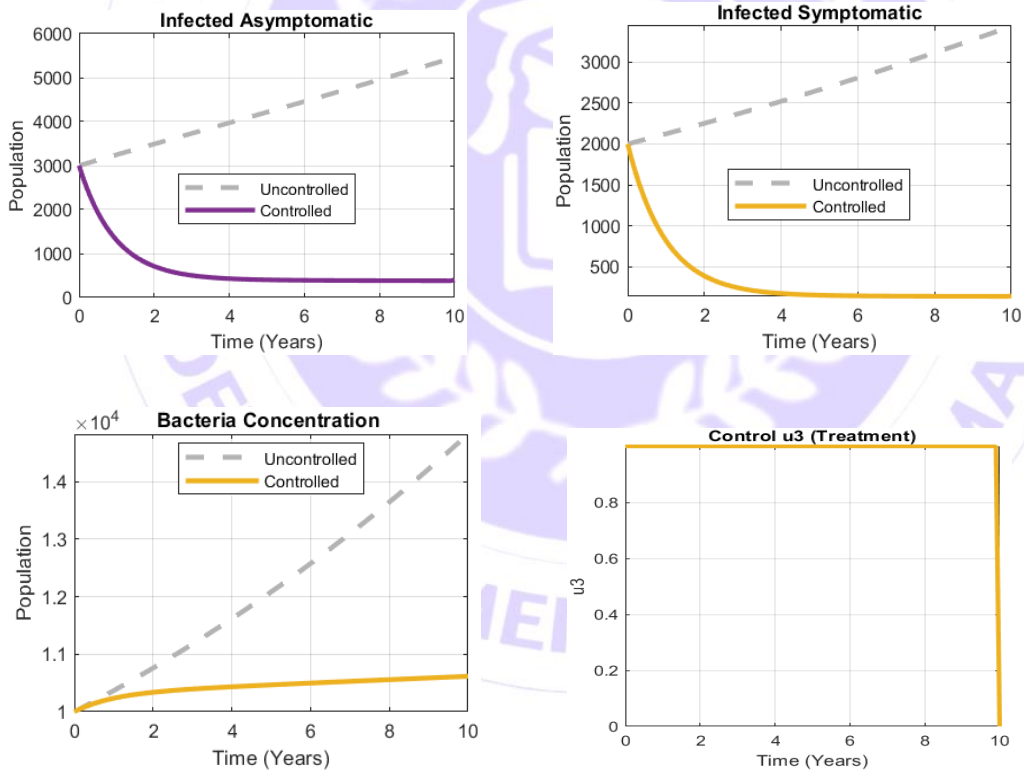

Figure 11. Numerical simulation showing impact of u_3 on the infectious and bacteria population

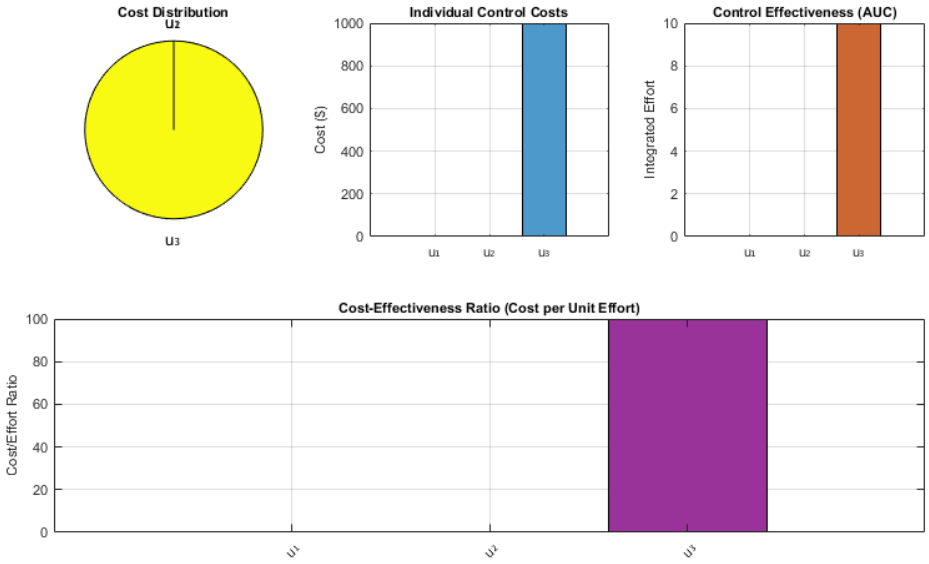

Figure 12. Numerical simulation showing the cost effectives of u_3 .

Figure 11 demonstrate that without treatment control (u_3), the asymptomatic population's increases, indicating persistent transmission, but with, (u_3) treatment it the population significantly reduces by controlling bacterial shedding. Symptomatic infections increases without intervention, signifying an uncontrolled epidemic, while with treatment shows a notable decrease in infections, approaching elimination. Furthermore, bacterial concentration in the aquatic environment increases from infected individuals, but with u_3 control it's stabilize these levels, highlighting the importance of addressing infections to reduce pathogen excretion. The optimal control trajectory for treatment requires maximum initial effort to suppress transmission effectively, followed by a decline as infections decrease. Early aggressive intervention is crucial for epidemic control, while sustained high treatment coverage is necessary for long-term stability. In Figure 12, the pie chart shows that 100% of the implementation cost goes to treatment. The cost bar chart illustrates that u_3 bears the entire expense, reaching the highest cost level in the system. This indicates the heavy financial burden of relying only on medical strategies. The Area under the curve chart reveals that treatment alone can significantly lower the disease burden by directly reducing the number of infections, highlighting u_3 strong control effect. The cost-effectiveness plot displays u_3 moderate CER value, showing that it is effective but also costly compared to preventive or isolation measures. This suggests that its short-term impact is less favorable.

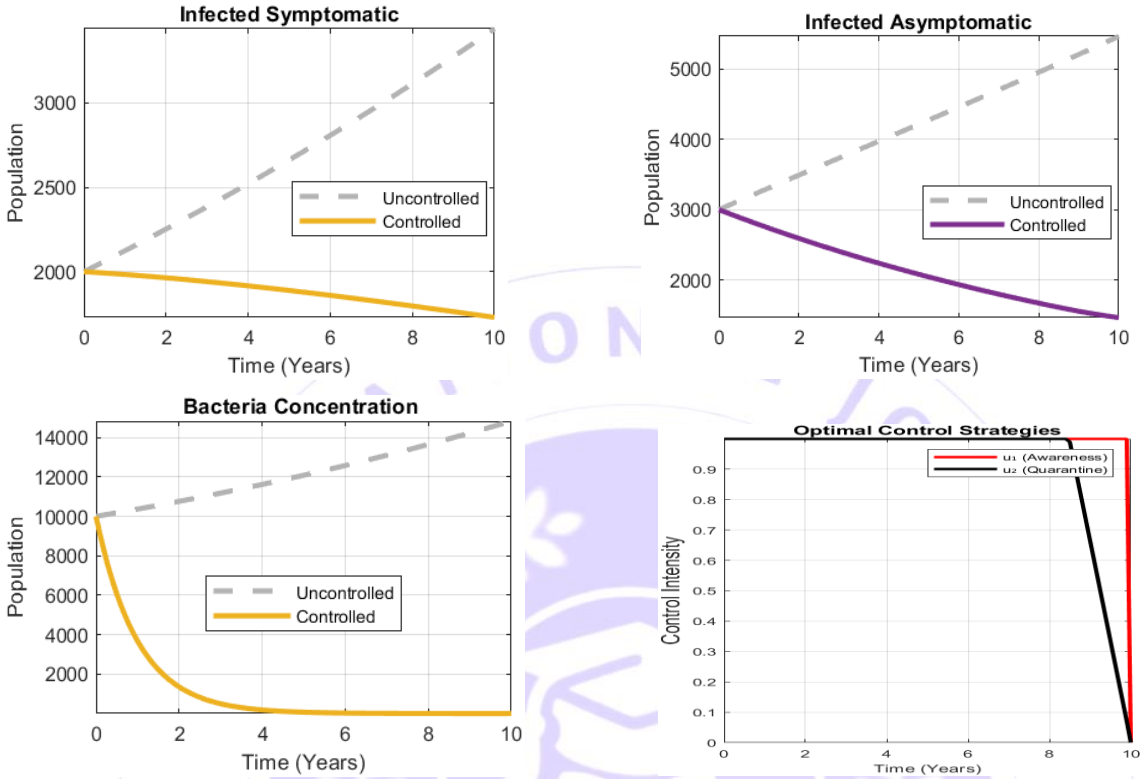

Figure 13. Numerical simulation showing impact of u_1 and u_2 on the infectious and bacteria population

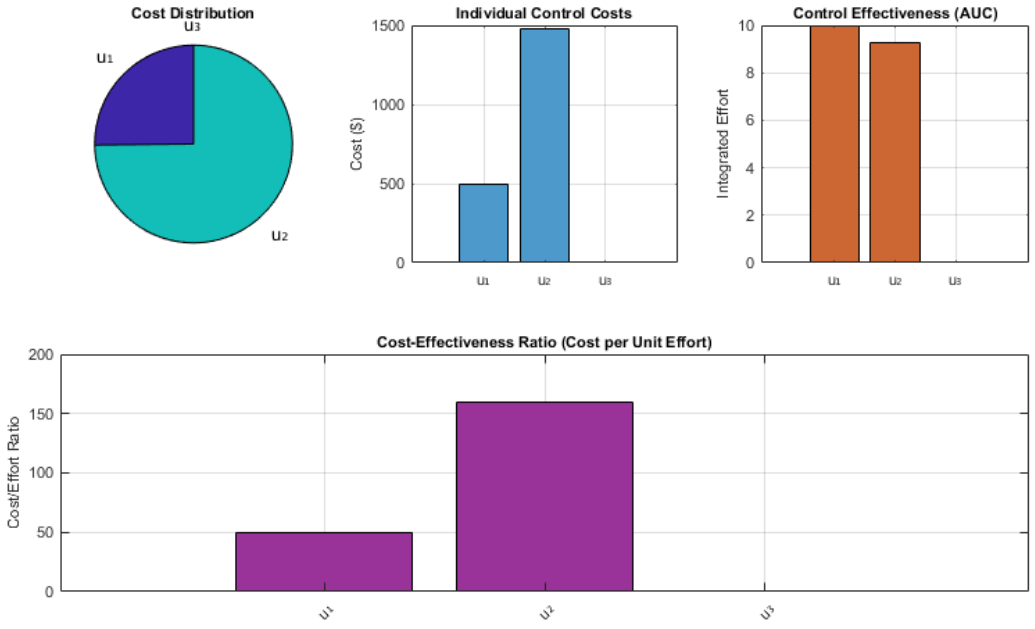

Figure 14. Numerical simulation showing the cost effectives of u_1 and u_2

Figure 13, depicts the combined effect of awareness (u_1) and quarantine (u_2) control strategies on cholera model 1.1 over a 10-year period. In scenarios without control measures, both symptomatic and asymptomatic infections increase, leading to epidemic growth, but employing both control strategies significantly reduces these populations and bacterial concentration in the environment, approaching zero levels. Awareness strategies (u_1), which remain maximized throughout the study, emphasize the need for ongoing health education and sanitation. In contrast, quarantine (u_2) measures are crucial during outbreak peaks but can be relaxed as infections decline. The findings indicate that the synergistic enforcement of awareness and quarantine is essential for effective cholera prevention and control, emphasizing the importance of public education and prompt quarantine measures. In Figure 14, the pie chart shows that quarantine-based interventions are the most cost-effective. The bar chart indicates that u_2 carries the highest total cost, while u_1 is the least expensive intervention. The Area under the curve plot indicates that u_1 and u_2 are highly effective when used together. However, their overall system effectiveness drops, which impacts the overall effectiveness of the control strategy over time. The cost-effectiveness ratio chart shows that u_1 is the most economical intervention, while u_2 has a higher cost-effectiveness ratio due to lower efficiency.to deliver high value for low cost, the overall cost-effectiveness of the control program worsens without $u's$ contribution to sustained infection reduction

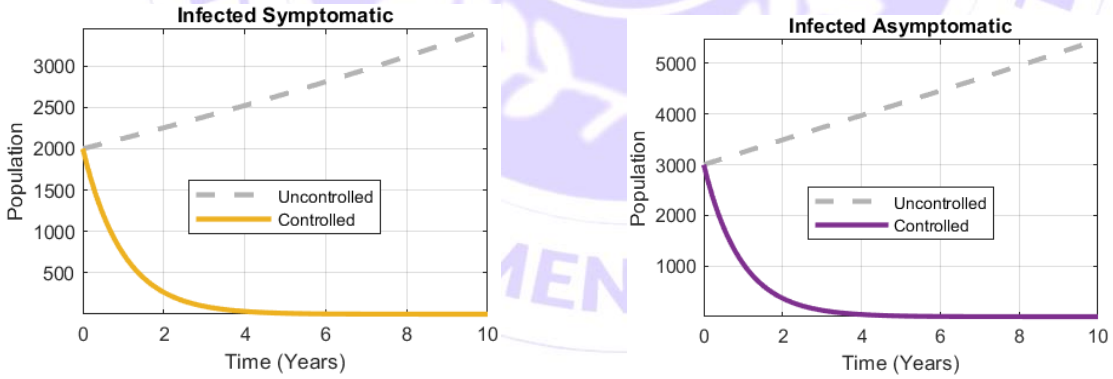

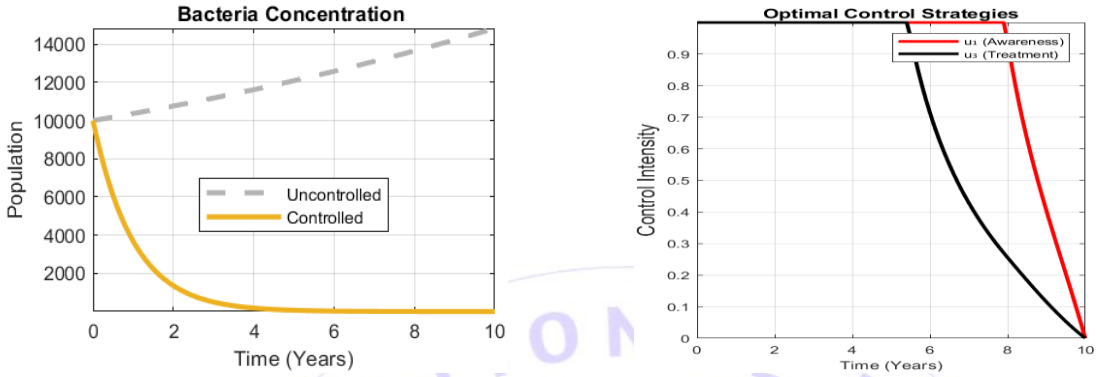

Figure 15. Numerical simulation showing impact of u_1 and u_3 on the infectious and bacteria population

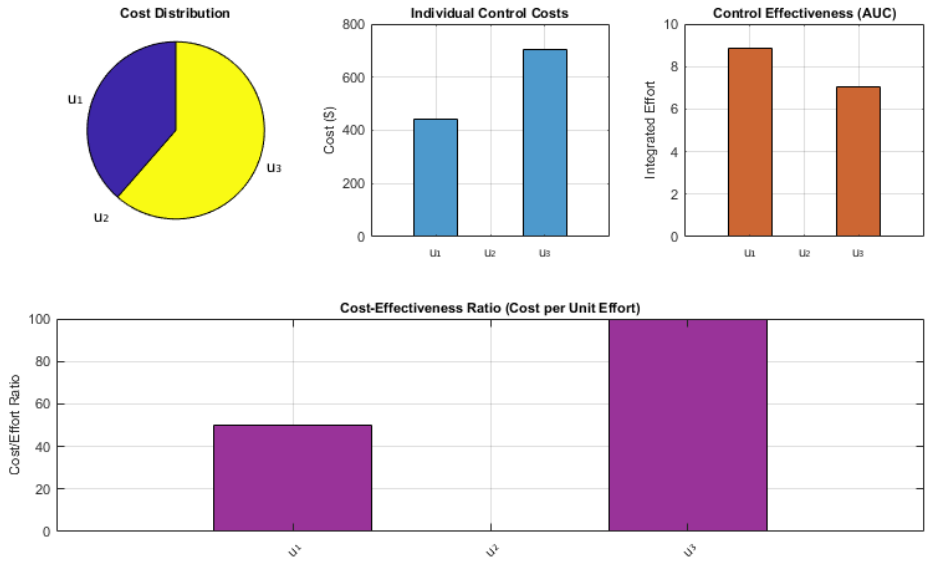

Figure 16. Numerical simulation showing the cost effectives of u_1 and u_3

In this scenario as depicted in Figure 15, we examines the joint impact of u_1 and u_3 controls on cholera transmission dynamics through numerical simulations over a 10-year period. The plots indicate that without interventions, both symptomatic and asymptomatic infections rise, maintaining high environmental bacterial levels. However, simultaneous implementation of u_1 and u_3 controls leads to a rapid decline in symptomatic infections and a gradual reduction in asymptomatic cases, with a significant drop in bacterial concentration indicating effective interruption of the infection cycle. The optimal control profiles reveal that u_1 efforts be maximizes and sustained over time, while

u_3 intensity should be high initially and reduced as infection rates decrease. This combined strategy is shown to be synergistic and cost-effective, minimizing disease prevalence and environmental contamination, thus supporting long-term cholera elimination goals. The pie chart shows that the total cost is divided between u_1 (education/awareness controls) and u_3 (treatment control). Treatment interventions make up the largest financial portion. The bar chart indicates that u_3 has the highest implementation cost, while u_1 remains the most affordable. The Area under the curve (AUC) plots demonstrate that both u_1 and u_3 play significant roles in reducing infections, with u_3 slightly outperforming u_1. This suggests that u_1 and u_3 control are effective over longer periods. The CER plot shows that u_1 is the cheapest control measure, while u_3 has a higher CER due to its greater expenses, as depicted in Figure 16.

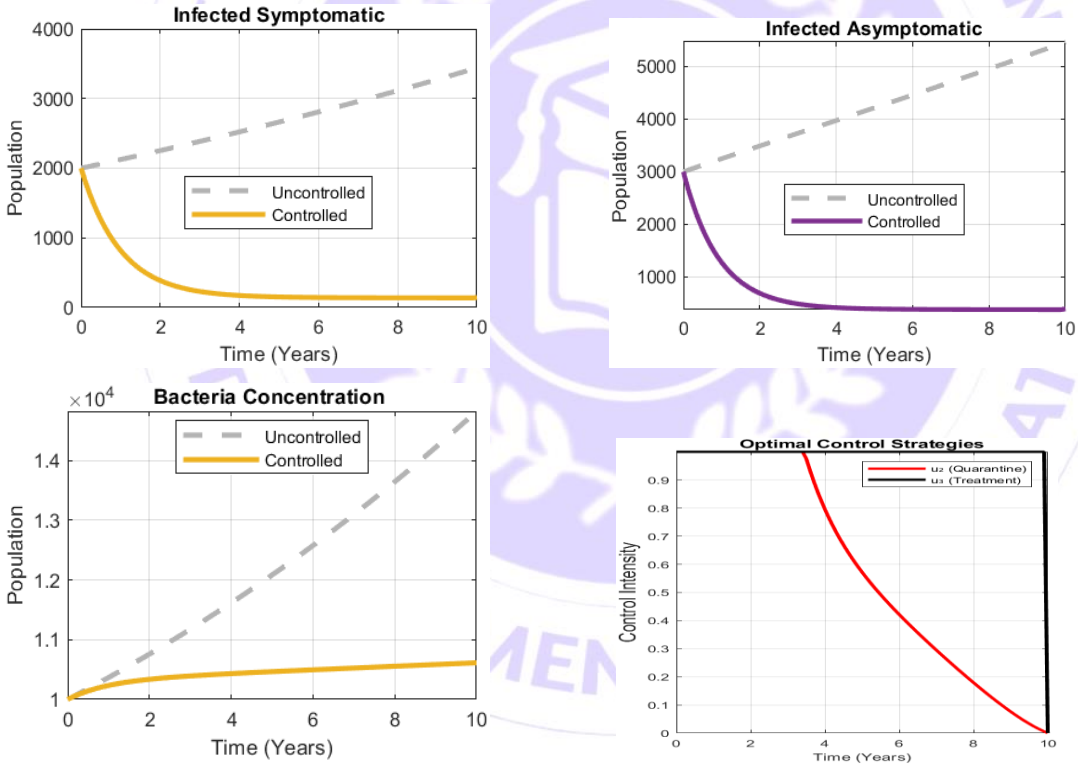

Figure 17. Numerical simulation showing impact of u_2 and u_3 on the infectious and bacteria population

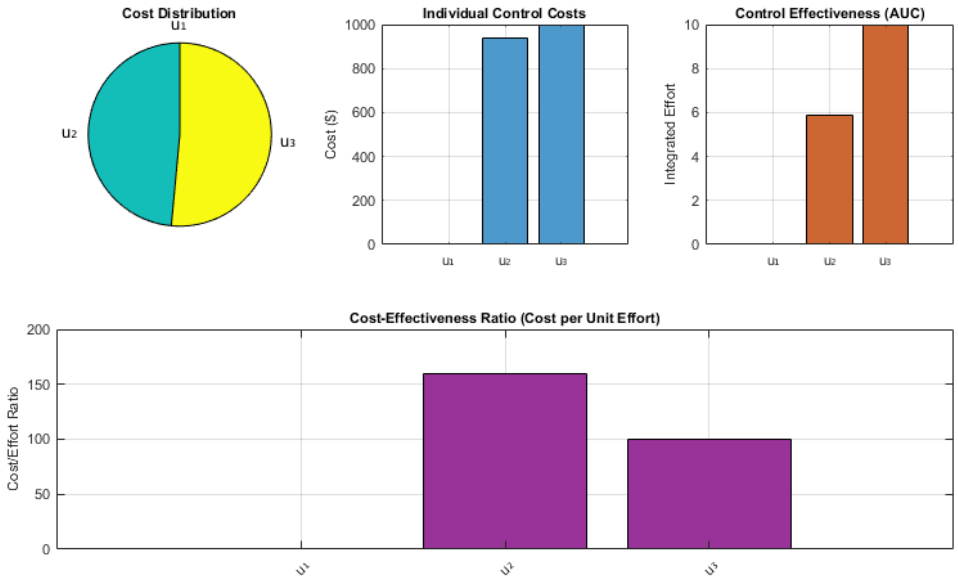

Figure 18. Numerical simulation showing the cost effectives of u_2 and u_3

In this scenario as depicted in Figure 17, we study the combined effects of u_2 and u_3 controls. Without controls, it is noticed that both symptomatic and asymptomatic infections rise, increasing environmental bacterial concentration and cholera spread. The simultaneous application u_2 and u_3 significantly reduces both populations, nearly eliminating symptomatic cases and lowering bacterial levels in the environment, thus breaking the transmission cycle. Furthermore, the Bacteria concentration is reduced compared to when there is no control. This combined approach proves to be a synergistic and effective strategy for cholera containment, stressing the necessity for early quarantine enforcement and ongoing treatment programs for sustainable control and eradication.

The pie chart indicates that implementation costs are mainly split between u_2 and u_3. u_2 makes up a larger share, showing that reactive measures are more effective in reducing infections. The bar chart reveals that both quarantine and treatment interventions incur significant costs, with quarantine being slightly more expensive because it requires more resources. The effectiveness plot shows that treatment (u_3) is better than (u_2) at reducing infection rates and bacterial levels, while u_2 has a moderate effect (AUC). The cost-effectiveness plot identifies u_2 as the least cost-effective control. In contrast, u_3 provides greater public health benefits for each dollar spent, making treatment the preferred option when prevention isn't possible as shown in figure 18.

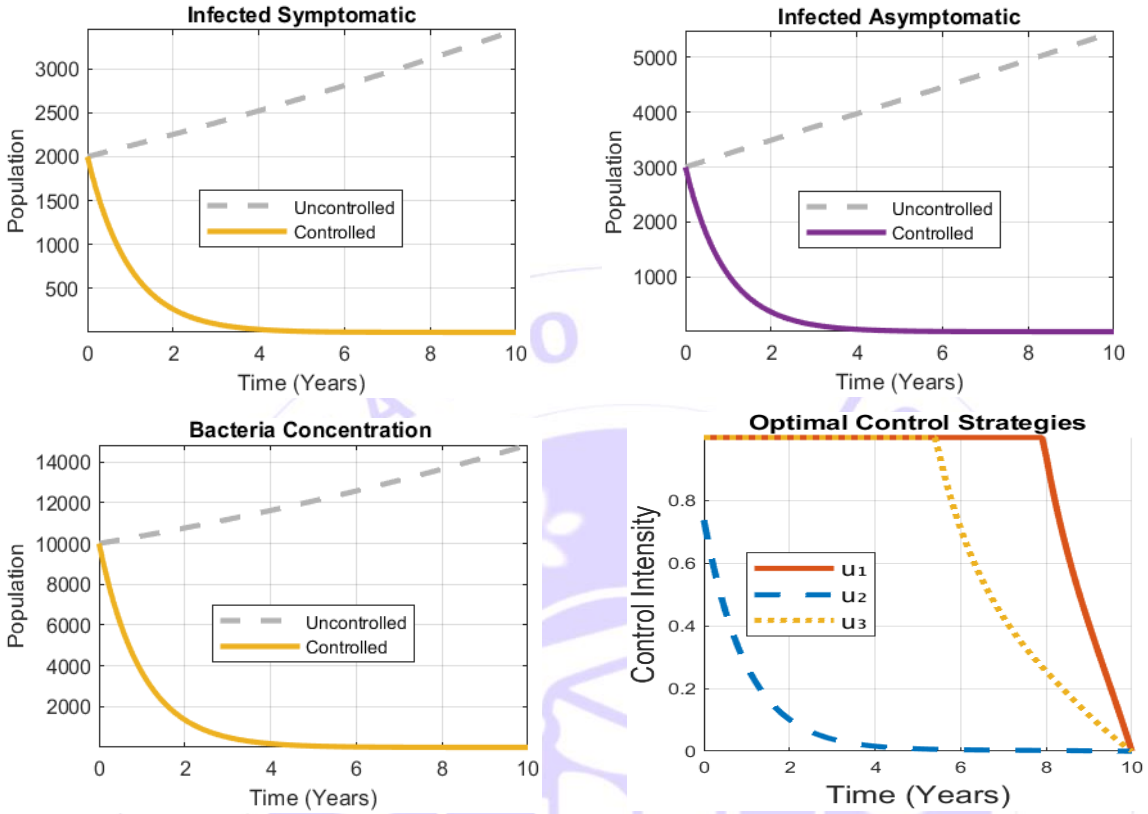

Figure 19. Numerical simulation showing impact of u_1, u_2 and u_3 on the infectious and bacteria population

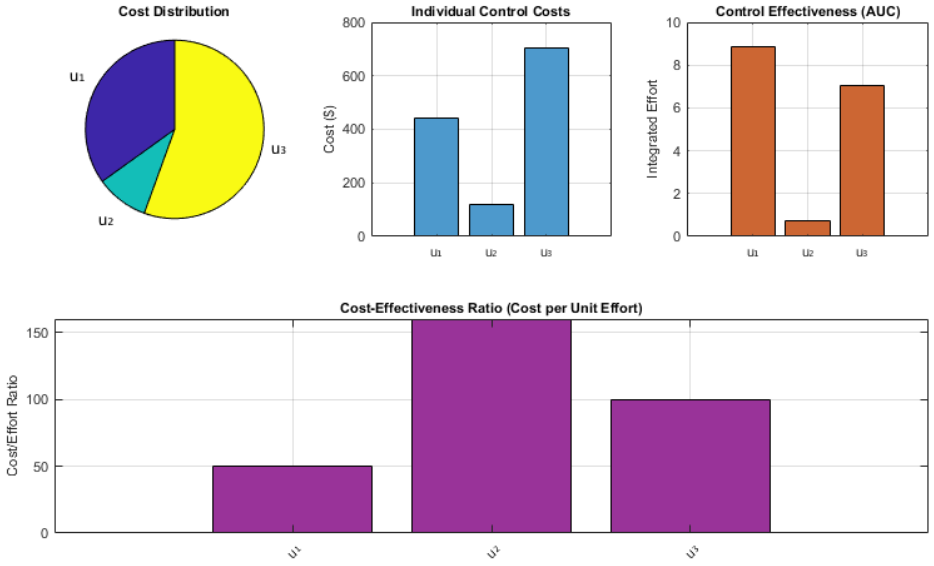

Figure 20. Numerical simulation showing the cost effectives of u_1, u_2 and u_3

The plot in figure 19, shows that without controls, symptomatic infection population's increase, indicating an uncontrolled epidemic. However, with combined control measures, they decline sharply, reaching near elimination within years. The asymptomatic infection class also shows a decline, with awareness campaigns and quarantine strategies effectively minimizing hidden transmission routes, reducing the overall infection reservoir. The plot shows that uncontrolled bacterial populations grow rapidly, reaching over 14,000 by year 10. Using optimal control strategies lowers bacterial levels and prevents long-term persistence, which proves their effectiveness. The figures illustrates the development of three control strategies, u_1, u_2 and u_3, which represent public awareness/education, quarantine and treatment. u_1 starts strong and decreases after control, u_2 remains low, and u_3 is moderate, striking a balance between prevention and stability. The cost distribution shows that treatment (u_3) require the most resources, but they are crucial for long-term sustainability. Treatment interventions (u_3) also account for the largest share of total control costs, followed by u_1, while u_2 incurs the least expense. The analysis reveals that u_3 has the highest total cost, while u_2 has the lowest, reflecting the trade-off between short-term and long-term strategies (AUC). The effectiveness plot indicates that u_1 and u_3 greatly influence infection reduction, while u_2 has a minimal impact, highlighting their roles in significant public health improvements. The cost-effectiveness ratio shows the economic efficiency of each control, with u_1 being the most economical, u_3 being the priciest, and u_2 being moderately efficient (as depicted in Figure 20).

5. Conclusion

This study developed and examined a comprehensive optimum control model for the spread of cholera that incorporates environmental, behavioral, and medicinal interventions. The results show that awareness, quarantine, and treatment controls, by concurrently reducing symptomatic and asymptomatic infections, as well as lowering environmental bacterial concentrations, are capable of efficiently reducing cholera outbreaks. Public awareness u_1 was the most cost-effective and long-lasting intervention among the interventions, which was mainly achieved through risk communication and hygiene promotion. Treatment, u_3 guarantees a quicker recovery and lessens bacterial shedding, while quarantine u_2, increases awareness by preventing direct transfer from infected people. Infection is almost completely eradicated in just a few years, illustrating the need for comprehensive community-based public health initiatives. This study was able to emphasize the importance of consistent public education, prompt medical

intervention, and effective quarantine enforcement as a comprehensive strategy for cholera control. The results also highlighted the necessity for cost-optimized multi-intervention strategies for long-term disease control, especially in low resource areas where cholera is still endemic. The results assist in informing national and regional cholera initiatives cost-effectively and are also aligned with the WHO Global Roadmap to End Cholera by 2030.

Reference

Abdulrahim, A., Ibrahim, M. N., \& Gulumbe, B. H. (2024). Cholera emergency in Nigeria: urgent need for better vaccine access and public health action. *Bulletin of the National Research Centre/Bulletin of the National Research Center*, *48*(1). https://doi.org/10.1186/s42269-024-01242-x.

Al-Arydah, M., Mwasa, A., Tchuenche, J. M., & Smith, R. J. (2013). Modeling Cholera Disease with Education and Chlorination. *Journal of Biological Systems*, *21*(04), 1340007. https://doi.org/10.1142/s021833901340007x.

Al-Shanfari, S., Elmojtaba, I. M., Al-Salti, N., & Al-Shandari, F. (2024). Mathematical analysis and optimal control of cholera–malaria co-infection model. *Results in Control and Optimization*, *14*, 100393. https://doi.org/10.1016/j.rico.2024.100393.

Amadi, P., Lawı, G., & Bonyo, J. (2024). A Metapopulation Model for Cholera with Variable Media Efficacy and Imperfect Vaccine. Journal of Mathematical Sciences and Modelling, 7(1), 20-32. https://doi.org/10.33187/jmsm.1289684

Anteneh, L. M., Zanvo, S. D., Traore, K., & Kakaï, R. G. (2025). Modelling the Impact of Vaccination on Cholera Transmission Dynamics under Stratified Populations and Seasonality. *Infectious Disease Modelling*, *10*(4), 1138–1152. https://doi.org/10.1016/j.idm.2025.06.006

Berhe, H. W. (2020). Optimal control strategies and cost-effectiveness analysis applied to real data of cholera outbreak in Ethiopia's Oromia region. *Chaos Solitons & Fractals*, *138*, 109933. https://doi.org/10.1016/j.chaos.2020.109933.

Cai, L., Tuncer, N., & Martcheva, M. (2017). How does within-host dynamics affect population-level dynamics? insights from an immuno-epidemiological model of malaria. Mathematical Methods in the Applied Sciences, 20:6424–6450

Cui, X., Xue, D., & Pan, F. (2022). A fractional SVIR-B epidemic model for Cholera with imperfect vaccination and saturated treatment. *The European Physical Journal Plus*, *137*(12). https://doi.org/10.1140/epjp/s13360-022-03564-z

Driessche, P., & Watmough, J. (2002). Reproduction numbers and sub-threshold endemic equilibria for compartmental models of disease transmission. *Mathematical Biosciences*, 180, 29e48

Hezam, I. M., Foul, A., & Alrasheedi, A. (2021). A dynamic optimal control model for COVID-19 and cholera co-

infection in Yemen. *Advances in Difference Equations*, *2021*(1). https://doi.org/10.1186/s13662-021-03271-6.

King, A. A., Ionides, E. L., Pascual, M., \& Bouma, M. J. (2008). Inapparent infections and cholera dynamics. *Nature*, *454*(7206), 877–880. https://doi.org/10.1038/nature07084

Lakshmikantham, V., Leela, S., & Martynyuk, A. A. (2015). Stability analysis of nonlinear systems. In *Systems & control*. https://doi.org/10.1007/978-3-319-27200-9.

LaSalle, J. P. & Lefschetz, S. (1961). *Stability by Lyapunov's Second Method with Applications.* New York: Academic Press.

Lemos-Paião, A. P., Silva, C. J., & Torres, D. F. (2016). An epidemic model for cholera with optimal control treatment. *Journal of Computational and Applied Mathematics*, *318*, 168–180. https://doi.org/10.1016/j.cam.2016.11.002

Lenhart, S. and Workman, J.T. (2007) *Optimal Control Applied to Biological Models. Mathematical and Computational Biology Series*, Chapman & Hall/CRC, London

Maity, B., Banerjee, S., Senapati, A., Pitchford, J., & Chattopadhyay, J. (2025). Coupling plankton and cholera dynamics: Insights into outbreak prediction and practical disease management. *PLoS Computational Biology*, *21*(9), e1013523. https://doi.org/10.1371/journal.pcbi.1013523.

Momoh, A. A., Abdulwasiu, G., Modu, G. U., Onimode, B. M., Ahmed, I., Abubakar, A., & Tariboon, J. (2025). Controlling the Spread of Malaria-Cholera Co-infection with Effective Intervention Strategy. *Bangmod International Journal of Mathematical and Computational Science*, *11*, 75–107. https://doi.org/10.58715/bangmodjmcs.2025.11.5.

Mustapha, U. T., Maigoro, Y. A., Yusuf, A., & Qureshi, S. (2024). Mathematical modeling for the transmission dynamics of cholera with an optimal control strategy. *Bulletin of Biomathematics*. https://doi.org/10.59292/bulletinbiomath.2024001.

Mukandavire, Z., Liao, S., Wang, J., Gaff, H., Smith, D. L., & Morris, J. G. (2011). Estimating the reproductive numbers for the 2008–2009 cholera outbreaks in Zimbabwe. *Proceedings of the National Academy of Sciences*, *108*(21), 8767–8772. https://doi.org/10.1073/pnas.1019712108.

Nelson, Metet K., Wasike A.M. Adu, Njuguna Edward, & Makwata Harun. (2025). “Mathematical Modelling of Cholera Transmission Dynamics Incorporating Vaccination”. Asian Research Journal of Mathematics 21 (4): 182-95. https://doi.org/10.9734/arjom/2025/v21i4921.

Neilan, R. L. M., Schaefer, E., Gaff, H., Fister, K. R., & Lenhart, S. (2010). Modeling optimal intervention strategies

for cholera. *Bulletin of Mathematical Biology*, *72*(8), 2004–2018. https://doi.org/10.1007/s11538-010-9521-8.

Ogunniyi, T.J., Muoneke, A.P., Nimo, F., Yisa, S. S., \& Olorunfemi, T. O. (2025). Cholera in Nigeria: a five-decade review of outbreak dynamics and health system responses. *J Health Popul Nutr* **44**, 329. https://doi.org/10.1186/s41043-025-01096-7

Posny, D., Wang, J., Mukandavire, Z., & Modnak, C. (2015). Analyzing transmission dynamics of cholera with public health interventions. *Mathematical Biosciences*, *264*, 38–53. https://doi.org/10.1016/j.mbs.2015.03.006

Sanda, A., Odekunle, M. R., Dione, D., & Momoh, A. A. (2024). Modeling and Stability Analysis of Fractional Human African Trypanosomiasis Dynamics with Optimal Control. *Journal of Mathematical Sciences*. https://doi.org/10.1007/s10958-024-07413-5

Song, C., Xu, R., Bai, N., Tian, X., & Lin, J. (2020). Global dynamics and optimal control of a cholera transmission model with vaccination strategy and multiple pathways. *Mathematical Biosciences & Engineering*, *17*(4), 4210–4224. https://doi.org/10.3934/mbe.2020233.

Wang J. (2022). Mathematical Models for Cholera Dynamics-A Review. *Microorganisms*, *10*(12), 2358. https://doi.org/10.3390/microorganisms10122358

Wang, X., & Wang, J. (2014). Analysis of cholera epidemics with bacterial growth and spatial movement. *Journal of Biological Dynamics*, *9*(sup1), 233–261. https://doi.org/10.1080/17513758.2014.974696.

WHO (2022). Cholera vaccines: WHO position paper. Weekly Epidemiological Record, 97(25), 317–340.

World Health Organization. (2017). *Ending cholera: A global roadmap to 2030*. Global Task Force on Cholera Control (GTFCC). World Health Organization. https://www.who.int/publications/i/item/ending-cholera-a-global-roadmap-to-2030.

Yang, C., Wang, X., Gao, D., & Wang, J. (2017). Impact of awareness programs on cholera dynamics: Two modeling approaches. *Bulletin of Mathematical Biology*, *79*(9), 2109–2131. https://doi.org/10.1007/s11538-017-0322-1

Zheng, Q., Luquero, F. J., Ciglenecki, I., Wamala, J. F., Abubakar, A., Welo, P., Hussen, M., Wossen, M., Yennan, S., Keita, A., Lessler, J., Azman, A. S., & Lee, E. C. (2022). Cholera outbreaks in sub-Saharan Africa during 2010-2019: a descriptive analysis. International Journal of Infectious Diseases, 122, 215–221. https://doi.org/10.1016/j.ijid.2022.05.039.